Multi-channel *in situ* dynamic light scattering instrumentation enhancing biological small-angle X-ray scattering experiments at the PETRA III beamline P12

Authors

Sven Falke[a], Karsten Dierks[b], Clement Blanchet[c], Melissa Graewert[c], Florent Cipriani[d], Rob Meijers[c], Dmitri Svergun[c] and Christian Betzel[a]*

[a]Laboratory for Structural Biology of Infection und Inflammation, University Hamburg, c/o DESY, Building 22a, Notkestraße 85, Hamburg, 22603, Germany

[b] Xtal Concepts GmbH, Marlowring 19, Hamburg, 22525, Germany

[c] European Molecular Biology Laboratory (EMBL), Hamburg Outstation, c/o Notkestraße 85, Hamburg, 22607, Germany

[d] European Molecular Biology Laboratory (EMBL), 71 Avenue des Martyrs, Grenoble, 38042, France

Correspondence email: Christian.Betzel@uni-hamburg.de

Synopsis A novel *in situ* DLS module implemented at the PETRA III EMBL beamline P12 is capable to perform real time sample solution scoring in parallel to BioSAXS experiments, including a multi-channel DLS detection principle.

Abstract Small-angle X-ray scattering (SAXS) analysis of biomolecules is increasingly common with a constantly high demand for comprehensive and efficient sample quality control prior to SAXS experiments. As monodisperse sample suspensions are desirable for SAXS experiments, latest dynamic light scattering (DLS) techniques are most ideal to obtain non-invasive and rapid information about the particle size distribution of molecules in solution. A multi-receiver four-channel DLS system was designed and adapted at the BioSAXS end station of the EMBL beamline P12 at PETRA III (DESY, Hamburg, Germany). The system allows to collect DLS data within round-shaped sample capillaries used at beamline P12. Data obtained provide information about the hydrodynamic radius of biological particles in solution and dispersity of the solution. DLS data can be collected directly prior and during an X-ray exposure. To match the short X-ray exposure times of around 1 s for 20 exposures at P12, the so far used DLS data collection periods of 20 s or commonly more were substantially reduced, using a novel multi-channel approach collecting DLS data sets in the SAXS sample capillary at four different neighboring sample volume positions in parallel. The setup allows online scoring of sample solutions applied for SAXS experiments, supports SAXS data evaluation and for example indicates local inhomogenieties in a sample solution in a time-efficient manner.

Biological macromolecules with different molecular weights were applied to test the system and obtain information about the performance. All measured hydrodynamic radii are in good agreement with DLS results obtained by employing a standard cuvette instrument. Moreover, applying the new multi-channel DLS setup a reliable radius determination of sample solutions in flow, at flow rates normally used for size-exclusion chromatography-SAXS experiments, and higher flow rates was verified as well. We also show and confirm that the newly designed sample compartment with attached DLS instrumentation does not disturb SAXS measurements.

Keywords: *In situ* DLS; multi-channel radius determination; BioSAXS; sample compartment; sample quality assessment

1. Introduction

Dynamic light scattering (DLS), also called photon correlation spectroscopy is a powerful, highly adaptable and a widely used method to analyse the size distribution of various kinds of particles in solution [Minton, 2016], mostly measuring in cuvettes. Fields of application include size determination and quantification of macromolecules, viscosity determination of blood [Popov and Vitkin, 2016], optimizing solubility and homogeneity of biological samples, analysing dimensions and symmetry of particles [Schubert et al., 2015; Maes et al., 2015; Passow et al., 2015], determining the density of bacterial cultures [Loske et al., 2014], verification of pharmaceutical formulations [Fávero-Retto et al., 2013], support of three-dimensional *in vivo* imaging [Lee et al., 2012], time-resolved analysis of protein assembly or enzyme-catalysed reactions via monitoring changes of the particle size distribution [Georgieva et al., 2004; Yang et al., 2015; Liu et al., 2016]. Monitoring different stages of protein crystallization experiments applying *in situ* DLS methods is also possible [Meyer et al., 2012; Meyer et al., 2015; Schubert et al., 2017]. DLS is non-invasive and can be adapted to perform measurements *in situ* in a variety of sample containers, including capillaries to monitor for example counter diffusion crystallization experiments [Oberthuer et al., 2012]. In principle, the intensity fluctuations of coherent laser light scattered by particles, which undergo Brownian motion, are recorded over time at a specified angle. The fluctuations are correlated with itself after short time intervals and visualized as an intensity auto-correlation function (ACF) [Chu, 1970]. The ACF is evaluated by the CONTIN algorithm [Provencher, 1982] allowing to calculate the decay-time distribution of the particles in solution. Considering the viscosity and temperature of the solution, the Stokes-Einstein equation can be used to calculate the hydrodynamic radius (R_H).

DLS measurements were successfully applied to analyse sample solutions in flow at different stages of protein folding by Gast et al. in 1997. A particular fiber optic DLS probe was used by Leung et al. [2006] to characterize latex particles in flow, pointing at a variety of potential industrial applications

to count and determine the size of particles for quality control in flow. The application of DLS in a shear flow and in a microfluidic channel was mathematically described by Destremaut et al. [2009], taking the channel dimensions, shear rates, velocity profile of a Poiseuille flow and interferences of different Doppler shifts into account. The resulting theoretical approximation of an ACF with some geometrical restrains underlined that below a critical flow rate the ACF is dominated by Brownian motion of the scattering molecules. In summary, DLS techniques allow to analyse the homogeneity of sample solutions in a very time-efficient way and are highly sensitive towards detecting larger aggregates of biological macromolecules. This qualifies DLS to be an excellent method for sample quality verification prior or during Small-angle X-ray scattering (SAXS) experiments.

SAXS is a well-established method to analyse biological macromolecules in solution at the EMBL PETRA III beamline P12 (DESY, Hamburg) [Blanchet et al., 2015]. BioSAXS techniques are applied to analyse tertiary and quaternary structures or even time-resolved folding, degradation or complex formation of (biological) macromolecules in solution, utilizing X-ray scattering intensities pattern at small angles [Franke et al., 2012; Graceffa et al., 2013; Sviridova et al., 2017]. Applying *ab initio* modelling techniques the shape of macromolecules can be calculated [Tuukkanen et al., 2016; Franke et al., 2017]. At the BioSAXS beamline P12 data collection can be performed in batch or in flow mode. An automated data processing pipeline, including *ab initio* model building [Franke et al., 2012], allows a rapid data evaluation, providing information about shape, size and folding status of the samples. However, a pre-requirement for SAXS experiments usually is a monodisperse and well defined sample solution. In order to determine the dispersity of a solution prior to a SAXS experiment and to verify SAXS data DLS is a well-accepted method [Regini et al., 2010; Carvalho et al., 2014; Dahani et al., 2015; Khan et al., 2017]. A combined DLS-SAXS setup allows a direct cross-verification and calculation of the ratio of gyration radius (R_G) and R_H, i.e. the shape factor of macromolecules, described by Burchard [1996] and Frankema et al. [2002]. Moreover, any unfortunate effects of sample handling, storage and X-ray exposure causing polydispersity and aggregation of the sample solution can be monitored by DLS.

At the SAXS beamline P12 sample solutions are often flowing through a capillary to reduce radiation damage [Jeffries et al., 2015]. Sample solutions flowing through the sample container in a SAXS experiment are also common at other X-ray sources [Martin et al., 2016, Poulos et al., 2016]. To improve sample quality, many beamlines now offer a set-up which combines a SAXS sample chamber and a liquid-chromatography instrument, i.e. size-exclusion chromatography-SAXS (SEC-SAXS) [David and Pérez, 2009; Graewert et al., 2015], allowing in-flow SAXS measurements after final pre-separation and purification of particles by (size-exclusion) chromatography. Examples applying SEC-SAXS for membrane proteins [Berthaud et al., 2012] and nucleic acid complexes [Beckham et al., 2013] confirmed the performance and potential of the method. To further upgrade and optimize SAXS data collection at beamline P12 an advanced and so far unique DLS

instrumentation was designed, constructed and tested, allowing to measure DLS in cylindrical capillaries prior to SAXS measurements in batch and flow mode. The multi-channel setup allows to collect data by four individual autocorrelation units in parallel in order to reduce the time consume of the DLS experiment by a factor of four, which accommodates with typically very short X-ray exposure times at synchrotrons today. The non-invasive synchronized DLS measurements support data analysis of BioSAXS experiments. A set of different samples covering the range of molecular weight typically analysed at P12 was used to test the performance of *in situ* DLS in combination with SAXS measurements.

2. Material and Methods

2.1. SAXS and DLS sample environment

The EMBL BioSAXS beamline P12 is located at the PETRA III storage ring (DESY, Hamburg) and provides a beam focus of approx. 200 x 120 µm^2 (full width half maximum) and a flux of up to 10^{13} photons s^{-1} [Blanchet et al., 2015]. The energy is tuneable between 4 and 20 keV. Particular care has been taken to reduce background scattering and to allow efficient sample supply. The sample compartment (also called sample exposure unit, SEU) contains a particular flow-through glass capillary with a circular cross-section and an inner diameter of 1.7 mm held by a metal pod at both ends [Round et al., 2015]. The sample temperature can be regulated and controlled in a range of approx. 7 to 45 °C. The capillary can be connected either to a robotic sample changer [Round et al., 2015] or to a size exclusion column system [Graewert et al., 2015]. A CCD camera allows to monitor the sample capillary inside the SEU. To allow *in situ* DLS measurements in the standard sample environment the capillary holder, the design of the surrounding cooling block and the chamber were modified to provide appropriate holders for the optics as well as windowed cylindrical SEU pathways with a diameter of 5 mm for the primary DLS laser beam and for the photons scattered in the direction of the four detectors. The SEU was manufactured by Arinax (Moirans, France).

The DLS setup consists of four major components: a) laser source; b) optical elements defining the optimised scattering geometry; c) detector and correlator system and d) electronic units including a PC. The arrangement of these components is shown schematically in figure 1A. Laser source, detector and all electronic components are combined in a mobile cabinet. Optical fibers cables connect the optics attached to the sample chamber with laser and detector electronics in the cabinet. A laser diode provides a wavelength of 660 nm and 120 mW output power. An objective lens, a Faraday isolator and a focus optic is combined to guide the laser light into a single mode fiber cable. A set of precise adjustment screws ensures a stable and efficient coupling (supplied by Schäfter + Kirchhoff GmbH,

Germany). The laser light at the fiber output is focused into the SAXS sample capillary with a collimator of 50 mm focal length resulting in a minimal beam diameter of 25 µm inside the capillary. An adjustment mechanism similar to that of the laser source is installed to further align and focus the laser beam in the capillary. The light scattered by the sample in the capillary is focused towards four receiver fibers with achromatic lenses. A modified optical fiber connector with a specially designed ferrule is in use to align the ends of these four fibers next to each other in a single row. The scattered light emerging from equidistant points along the laser beam passage within the sample solution is thus collected by the four fibers. Single-mode fibers with 4.6 µm core diameter were used, which transfer the light to fibers with 50 µm core diameter linked to the photomultiplier modules. Figure 1B shows the beam passage of the laser beam through a sample suspension inside the SAXS capillary. A rotable x/y-translation stage allows precise alignment of the four receiver focus points. Each fiber cable is connected to an individual photomultiplier module (Hamamatsu H10682, Hamamatsu, Japan). The corresponding output signals are transferred to four correlator units (Xtal Concepts, Germany), which subsequently transfer data to a PC for further analysis (Design of optics and DLS instrumentation by Xtal Concepts). The correlators are capable to process interval times between 400 ns and several seconds to calculate ACFs. As a result, sample particle sizes ranging from R_H = 0.8 nm up to approx. 100 µm can be measured and analysed. Also, the DLS data generated can be further individually processed for statistical analysis and individual display.

The SEU CCD camera can monitor the laser beam passage through the capillary and the section of the capillary utilized for light scattering, with one light scattering section overlapping the X-ray beam pass. For flow experiments an HPLC pump (Viscotek, Malvern, UK) together with flexible tubes is attached to the capillary holder allowing linear or circular flow. A 0.22 µm cellulose acetate filter eliminates remaining larger particles or impurities. For chromatographic test experiments the HPLC pump tubing was connected to a size-exclusion column, i.e. Superdex 200 5/150 GL or Superdex 200 10/300 GL (GE Healthcare, USA) respectively, which is directly connected to the SAXS capillary for DLS measurements.

2.2. DLS data collection and processing

All experiments were carried out at room temperature. Standardised globular latex microspheres (Thermo Scientific, USA) were used first to verify the setup and comparative reference measurements of sample solutions were made with a cuvette DLS instrument (SpectroLight 300, Xtal Concepts, Germany). The intensity fluctuations of the scattered laser light, produced by the Brownian movement of the sample particles, were processed by the autocorrelation units and transformed to autocorrelation functions (ACFs). The program CONTIN [Provencher, 1982] calculates decay time constants from the ACFs and utilizes the Stokes-Einstein equation to directly calculate the hydrodynamic radius

distributions of the sample solutions. For CONTIN analysis of the ACF, 80 logarithmically scaled grid points in the range from 2 µs to 1 s were used. The calculated polydispersity index (PDI) represents the mean broadness of the peaks as directly identified via CONTIN analysis. The software package developed to operate the multi-channel *in situ* DLS instrument is able to process all data collected by four channels over a range of 650 µm of the inner capillary's diameter, which corresponds to approx. 40 % of the total capillary diameter, simultaneously (Figure 1B).

The calculated size distribution information is weighted by scattering intensity in all described experiments. Also the software also allows weighting by molecular weight of the particles. The size distribution is displayed as histogram plot, i.e. an plot accumulating the radius values detected in a set of individual experiments, or time-resolved radius distribution plot. The software provides options for remote operation to enable integration of the data operations tools and measured data into the data acquisition system of the beamline. Based on R_H the molecular mass of particles was approximated as described by Cantor and Schimmel [1980], assuming a globular shape.

2.3 SAXS data collection and processing

SAXS data were collected at an X-ray wavelength of 1.24 Å, a sample detector distance of 3.1 m, in air and applying a PILATUS 2M pixel detector. Each of 20 consecutive scattering patterns collected for each sample (or buffer) were recorded with an X-ray exposure time of 45 ms. Individual frames were plotted and averaged with subsequent subtraction of the buffer scattering using PRIMUSQT [Franke et al., 2017] as part of the ATSAS software suite, which also contains DAMMIF in order to perform *ab initio* modelling. Twenty buffer scattering frames before and after the respective sample exposure were averaged. The implemented software tools AutoRg and AutoGnom were applied to calculate the radius of gyration and the pair distance distribution functions for determining the dimensions of the molecule (maximum diameter, D_{max}). To compare the solution scattering of standard proteins to the scattering of known high-resolution X-ray structures from the protein data bank (pdb; www.rcsb.org), CRYSOL [Svergun et al., 1995] was used to calculate the respective fit function and χ^2-value.

2.4 Samples

The experiments were performed with latex nano particles and lauryl sulfobetain, with a set of different commercially available proteins, as bovine serum albumin (BSA), lysozyme, apoferritin, thyroglobulin, conalbumin, RNase A, a granulovirus, in house expressed and purified inosine 5'-monophosphate dehydrogenase (IMPDH) from *Trypanosoma brucei* (ε = 29840 M^{-1} cm^{-1}), and the translationally controlled tumour protein (TCTP) from *Arabidopsis thaliana* (ε = 22920 M^{-1} cm^{-1}). All protein samples were centrifuged applying a table top centrifuge (Eppendorf 5424 R) at 16000 g for

30 minutes prior to DLS and SAXS experiments. All sample, buffer solutions and conditions used for DLS and SAXS experiments are summarised in table 1.

Table 1 Samples applied for DLS measurements ordered by molecular weight.

Sample	MW [kDa] (monomer)	Organism/Source	Supplier	Buffer/solvent
Latex microspheres	-	Synthetic	Thermo	Water
Lauryl sulfobetain[1]	-	Synthetic	Fluka	Water
Granulovirus	-	-	Neudorff	Water
Lysozyme	14	Hen egg	Sigma	PBS
RNase A	14	Bovine pancreas	GE Healthcare	30 mM NaH_2PO_4, 300 mM NaCl, pH 7.0
TCTP[2]	19	*A. thaliana*	In-house	PBS
Apoferritin	19/21	Horse spleen	Sigma	50 mM Tris, 3 % (v/v) glycerol, pH 7.5
Papain	23	*C. papaya*	Applichem	PBS
IMPDH[3]	58	*T. brucei*	In-house	50 mM HEPES, 400 mM Imidazol, 1 mM DTT, pH 7.0
BSA[4]	66	Bovine serum	Sigma	50 mM HEPES, 100 mM NaCl, pH 7.5
Conalbumin	75	Chicken egg white	GE Healthcare	30 mM NaH_2PO_4, 300 mM NaCl, pH 7.0
Thyroglobulin	330	Bovine thyroid	GE Healthcare	30 mM NaH_2PO_4, 300 mM NaCl, pH 7.0

[1]Micelles of lauryl sulfobetain (*N*-dodecyl-*N*,*N*-dimethyl-3-ammonio-1-propanesulfonate); [2]*Arabidopsis thaliana* translationally controlled tumour protein, a conserved multi-fuctional protein in cell homeostasis (UniProt code: P31265); [3]*Trypanosoma brucei* inosine 5'-monophosphate dehydrogenase, involved in *de novo* synthesis of the nucleobase guanin (UniProt code: P50098); [4]Bovine serum albumin.

3. Results

3.1 DLS instrumentation

3.1.1 The DLS-SAXS Measuring Unit

The four-channel *in situ* DLS instrument (Figures 1A/B and 2A) was designed and constructed to allow a rapid scoring of sample suspensions and solutions during SAXS experiments, e. g. allowing to detect even minor protein aggregation. The scattering geometry was designed and tested with an offline setup. The arrangement of flange-mounted laser and detector optics, which are connected on opposite sides of the capillary, was constructed in such a way to minimize unwanted stray light, laser beam attenuation, to optimize sensitivity and scattering intensity as well as to still match all the restraints due to the ccd camera position, capillary pod, X-ray beam passage and sample tubing. The focal length on both sides was consequently adjusted to 50 mm and the resulting scattering angle to 69°. The laser beam passage through the capillary is shown in figure 1B. (The entire sample compartment with attached optical DLS components is shown in figure 2A/B). The laser beam is focused to a diameter of approx. 25 µm inside the sample solution.

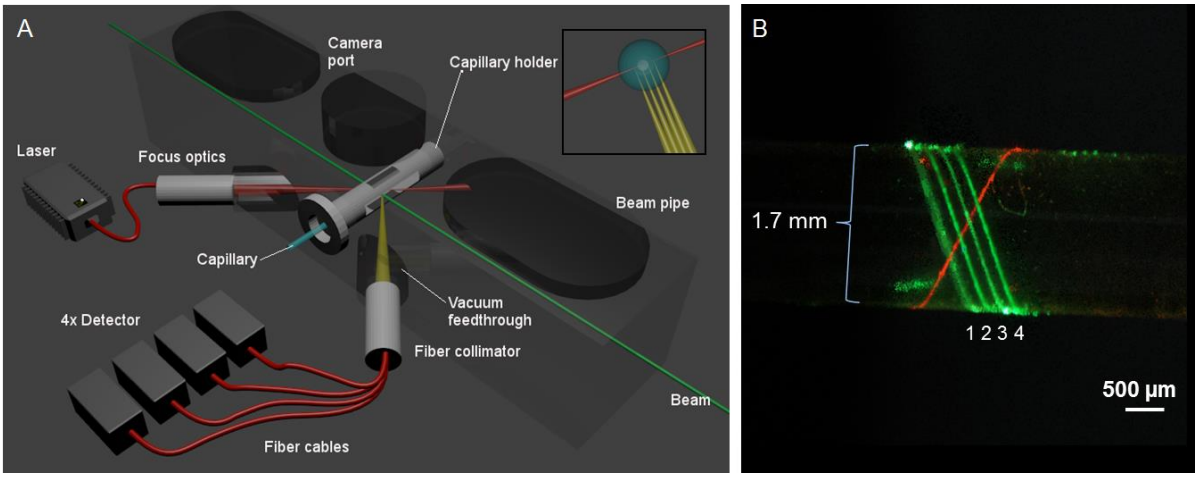

Figure 1 (**A**) Scheme of the four-channel *in situ* DLS instrument. The inset figure shows that the scattered light along the red laser beam is recorded close to its focal point in four statistically independent neighbouring volume fractions and guided to four individual autocorrelation units. (**B**) Image showing the DLS laser beam (red) in the SAXS capillary and green laser beams, coupled to the receiver fiber cables, indicating the path of scattered light towards the detector optics. The intercept points indicated the positions of the analysed volume fractions, which are separated from each other by approximately 200 µm.

The intercept points of the red DLS laser beam with each of the four aligned receiver fiber optics (indicated by green laser radiation) define the position or volume of the sample suspension that is scored, as visualized in figure 1B. The neighbouring sample volume fractions are separated by 200 µm from each other covering in total approx. 40 % of the capillary diameter in the center of the capillary. Four fiber cables are transmitting the scattered light to the corresponding autocorrelation units in parallel. The advanced correlator setup allows fast and reliable DLS measurements suitable with time intervals today typically used for X-ray exposures at the beamline P12 and other SAXS synchrotron beamlines located at 3rd generation synchrotrons.

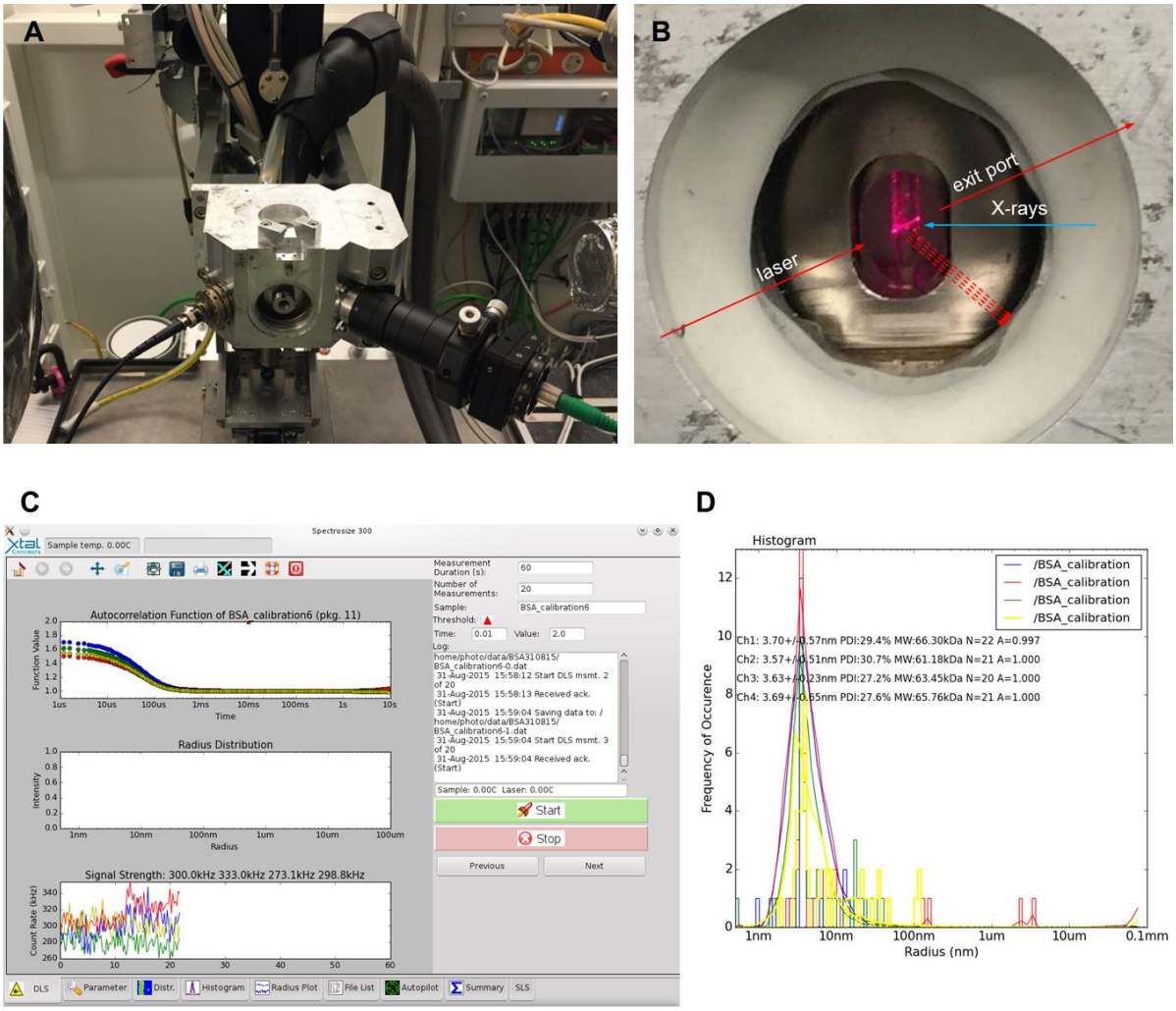

Figure 2 (**A**) DLS instrumentation attached to the SAXS sample exposure unit at beamline P12. The flange-mounted DLS laser and detection optics and fibers are located on opposite sides of the SEU. (**B**) Close-up image of the incident laser beam passing the sample solution inside the SAXS-SEU (top view). Scattered light in the direction of the detectors is symbolized by four red dashed lines. (**C**) Software window and a representative four-channel DLS measurement of BSA. The four data collection channels (ACF, count rate and histogram representation) are colour-coded in blue, red,

green and yellow in the order from 1 to 4. (**D**) Histogram presentation of the hydrodynamic radius distribution obtained for 9 mg ml^{-1} BSA solution in PBS. The hydrodynamic radius with the highest abundance in the averaged measurements is listed for each channel along with the PDI, derived from themean peak broadness resulting from CONTIN analysis. The molecular weight is estimated according to Cantor and Schimmel [1980], assuming a globular shape of the particle. Moreover, the abundancy of a radius value peak in the set of measurements (N) and the relative size of the peak area (A) are specified.

3.1.2. *In situ* DLS experiments in batch

In order to test and verify the *in situ* DLS instrument with four data collection channels, DLS data were collected first applying solutions of BSA (66 kDa) and lysozyme (14 kDa). BSA solutions are also commonly used for the molecular weight calibration of BioSAXS experiments. The DLS data were evaluated and an exemplary result is shown in figure 2C and D. The hydrodynamic radius determinations applying the four-channel *in situ* DLS system with 10 s data collection time for a single DLS measurement are summarized for a BSA solution in table 2 and for a lysozyme solution in table 3, respectively. The data correspond well to the hydrodynamic radius of BSA determined by Axelsson and Heinegård [1978] before to 3.5 nm and to the hydrodynamic radius of 2.1 nm for lysozyme as measured by Mikol et al., [1989].

Table 2 Radius values in nm for individual single measurements of 10 s each taken from a four-channel DLS experiment with BSA solution (9 mg ml^{-1}) in PBS (am: arithmetic mean of the respective measurements).

measurement	**1**	**2**	**3**	**4**	**5**	**6**
channel 1	3.95	3.76	4.00	3.94	3.46	3.93
channel 2	3.41	3.31	3.34	3.38	3.41	3.41
channel 3	3.76	3.61	3.80	3.58	3.44	3.62
channel 4	3.46	3.43	3.51	3.48	3.61	3.57
am (ch. 1-4)	**3.65 ± 7.0 %**	**3.53 ± 5.6 %**	**3.66 ± 8.0 %**	**3.60 ± 6.8 %**	**3.48 ± 2.6 %**	**3.63 ± 6.0 %**
measurement	**7**	**8**	**9**	**10**	**am (1-10)**	
channel 1	3.31	3.48	3.44	3.58	**3.69 ± 7.0 %**	
channel 2	3.36	3.28	3.43	3.39	**3.37 ± 1.5 %**	
channel 3	3.39	3.54	3.43	3.47	**3.56 ± 3.9 %**	
channel 4	3.26	3.47	3.55	3.56	**3.49 ± 2.8 %**	
am (ch. 1-4)	**3.33 ± 1.7 %**	**3.44 ± 3.3 %**	**3.46 ± 1.7 %**	**3.50 ± 2.5 %**	**3.53 ± 3.0 %**	

Table 3 Radius values in nm obtained for 10 individual single measurements of 10 s each, taken from a four-channel DLS experiment with lysozyme solution (16 mg ml^{-1}) in PBS (am: arithmetic mean of the respective measurements).

measurement	**1**	**2**	**3**	**4**	**5**	**6**
channel 1	2.56	1.96	1.95	1.95	2.16	2.18
channel 2	2.20	2.10	1.93	2.00	2.09	2.07
channel 3	2.24	2.21	2.05	2.05	2.09	2.09
channel 4	2.14	2.18	1.83	1.87	1.92	2.12
am (ch. 1-4)	**2.29 ± 8.2%**	**2.11 ± 5.3 %**	**1.94 ± 4.6 %**	**1.97 ± 3.9 %**	**2.07 ± 4.9 %**	**2.12 ± 2.2 %**
measurement	**7**	**8**	**9**	**10**	**am (1-10)**	
channel 1	1.87	2.14	2.20	2.36	**2.13 ± 9.9 %**	
channel 2	2.18	2.31	2.11	1.92	**2.09 ± 5.8 %**	
channel 3	2.04	2.11	2.13	2.20	**2.12 ± 3.4 %**	
channel 4	1.90	1.88	1.84	2.00	**1.97 ± 6.7 %**	
am (ch. 1-4)	**2.00 ± 7.1 %**	**2.11 ± 8.3 %**	**2.07 ± 7.6 %**	**2.12 ± 9.4 %**	**2.08 ± 3.6 %**	

According to the collected DLS data (table 2/3) the standard deviation of DLS measurements of each individual data collection channel in a single 10 s DLS measurement is approx. ± 10 %, which is still in the same regime as for a SpectroLight 300 cuvette instrument and of course essentially depends also on the total data collection time, sample concentration, particle size and homogeneity of the sample solution.

Next, the hydrodynamic radii of selected standard proteins covering a broad molecular weight range were determined applying the four channel DLS system and are summarized in table 4. They were compared to the hydrodynamic radii of the same samples obtained by a standard cuvette DLS instrument. The R_H values obtained from the four channel *in situ* DLS instrument are in good agreement (within ± 5-10 % deviation) with the values determined by DLS measurements in a quartz cuvette.

Table 4 Experimentally determined hydrodynamic radii obtained applying different light scattering setups.

Sample	**Expected mass [kDa]**	**Reported radius R_H**	**Cuvette instrument [R_H, nm] (mass[1])**	***In situ* DLS, batch [R_H, nm]**	***In situ* DLS in flow, 200 µl min^{-1} [R_H, nm]**
Microsphere	-	10.5 ± 0.5 nm	10.0 ± 0.7 (0.7 MDa)	10.0 ± 0.6	10.0 ± 0.8
Lauryl sulfobetain	-	-	3.0 ± 0.1 (38 kDa)	3.2 ± 0.5	3.3 ± 0.4

Lysozyme	14	2.1[2]	2.1 ± 0.1 (18 kDa)	2.1 ± 0.2	2.0 ± 0.2
RNase A	14	1.9[3]	2.2 ± 0.1 (21 kDa)	2.0 ± 0.2	2.0 ± 0.3
TCTP	38 (dimer)	-	2.9 ± 0.3 (36 kDa)	3.3 ± 0.1	2.8 ± 0.3
BSA	66	3.5[4]	3.8 ± 0.1 (70 kDa)	3.5 ± 0.4	3.6 ± 0.5
Apoferritin	440 (24-mer)	7.1[5]	7.9 ± 0.3 (385 kDa)	7.8 ± 0.3	n. d.
Thyroglobulin	660 (dimer)	8.6[6]	8.9 ± 0.1 (496 kDa)	8.9 ± 0.4	n. d.
Granulovirus	> 10 MDa	-	158.4 ± 23.0 (> 10 MDa)	168.3 ± 11.5	n. d.

[1]theoretical approximation based on R_H and assuming a globular particle shape according to Cantor & Schimmel [1980]; [2]Mikol et al. [1989]; [3]Noeppert et al. [1996]; [4]Axelsson and Heinegård [1978]; [5]Wong et al. [1998]; [6]Edelhoch & Lippoldt [1960].

After confirming the size determination of different particles in a monodisperse solution, *in situ* DLS was used to analyze polydisperse, i.e. at least didisperse solutions to verify that inhomogeneities in SAXS sample solutions can be identified. Defined mixtures of the compactly folded and nearly globular proteins lysozyme (14 kDa) and BSA (66 kDa) in PBS were prepared in order to determine the particle size distribution of these solutions containing different molar ratios of both proteins by *in situ* DLS, as shown in figure 3. The results demonstrate that in a sample solution of lysozyme small quantities of a protein like BSA, which has an approximately five times higher molecular weight and accordingly also a higher particle volume, are detectable.

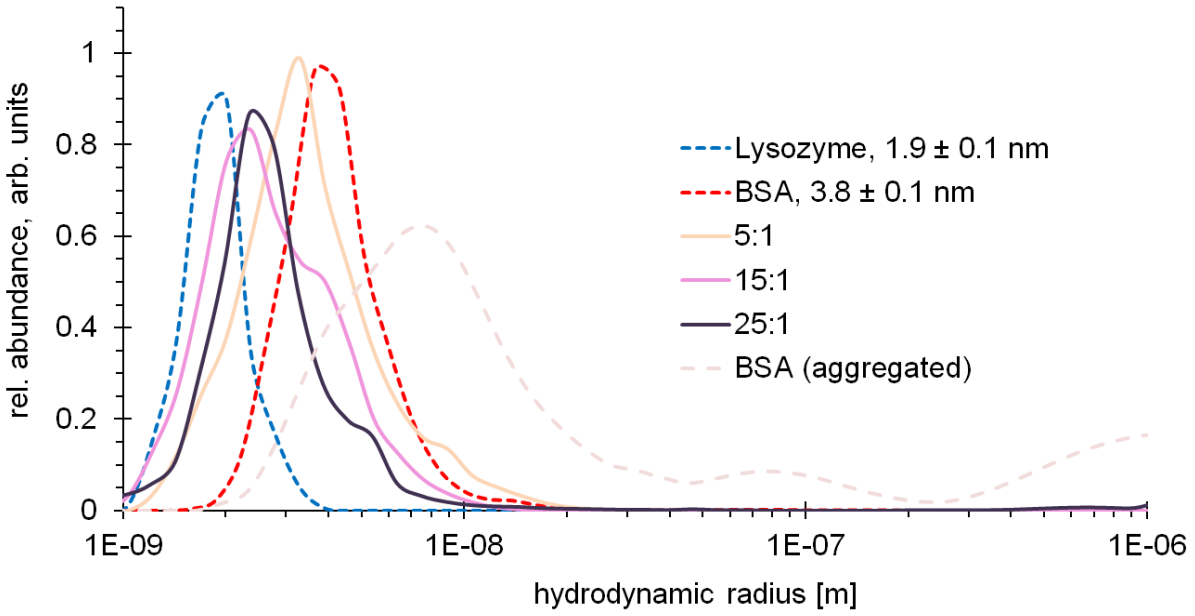

Figure 3 Radius distribution of pure freshly prepared lysozyme and BSA solutions as well as mixtures of lysozyme and BSA determined by *in situ* DLS. Solutions with different molar ratios (lysozyme : BSA) of both proteins were analysed by DLS for 10 s each and with up to 25-fold excess of lysozyme over BSA. Further, a highly polydisperse sample solution of aggregated BSA was measured after one month of storage at room temperature and is shown for comparison. A comparison of the radius distributions verifies the applicability of the *in situ* DLS instrument to identify and score inhomogenities and impurities in sample solutions.

3.1.3. *In situ* DLS experiments in flow

A large and increasing number of SAXS experiments are carried out in flow mode, i.e. the sample is flowing through the capillary. Therefore, *in situ* DLS experiments in nearly laminar flow were performed, applying first a test setup prior to the implementation of the DLS instrument at the SAXS beamline, as shown in figure 4. Using different flow rates suspensions of latex nano particles, BSA and lysozyme were used to analyze if velocity components of flowing suspensions influence DLS measurements and DLS data evaluation. A 2 ml suspension of synthetic latex particles (radius: 10.5 ± 0.5 nm) was injected into the sample capillary with a constant pump-driven velocity of 400 µl min^{-1} (Figure 4A; pump velocity shown in red). This flow rate corresponds to those often applied for SEC-SAXS experiments at beamline P12 and is typically not exceeded within the process of sample loading in other SAXS experiments. The pump was switched off after filling the capillary for five minutes. DLS measurements were performed continuously in parallel and the determined mean hydrodynamic radius of the sample particles was calculated to 10.5 ± 0.7 nm, confirming a reliable radius determination and the possibility to monitor the filling of the capillary in flow mode.

Moreover, BSA and lysozyme solutions were also analysed at different flow rates (Figure 4B). Consistent and comparable data were obtained for all four DLS channels, confirming that hydrodynamic radius determination based on Brownian motion is meaningful and can be performed at moderate flow rates. However, at flow rates above 2 ml min^{-1}, which corresponds to a particle movement of approx. 15 mm s^{-1} in the center of the capillary, a substantial decrease of the determined R_H was indicated. At these relatively high flow rates DLS measurements and the following R_H calculation are affected by a significantly increased particle diffusion coefficient. However, the experiments performed clearly demonstrate that sample flow rates typically used in SAXS experiments do not bias DLS measurements and the R_H determination.

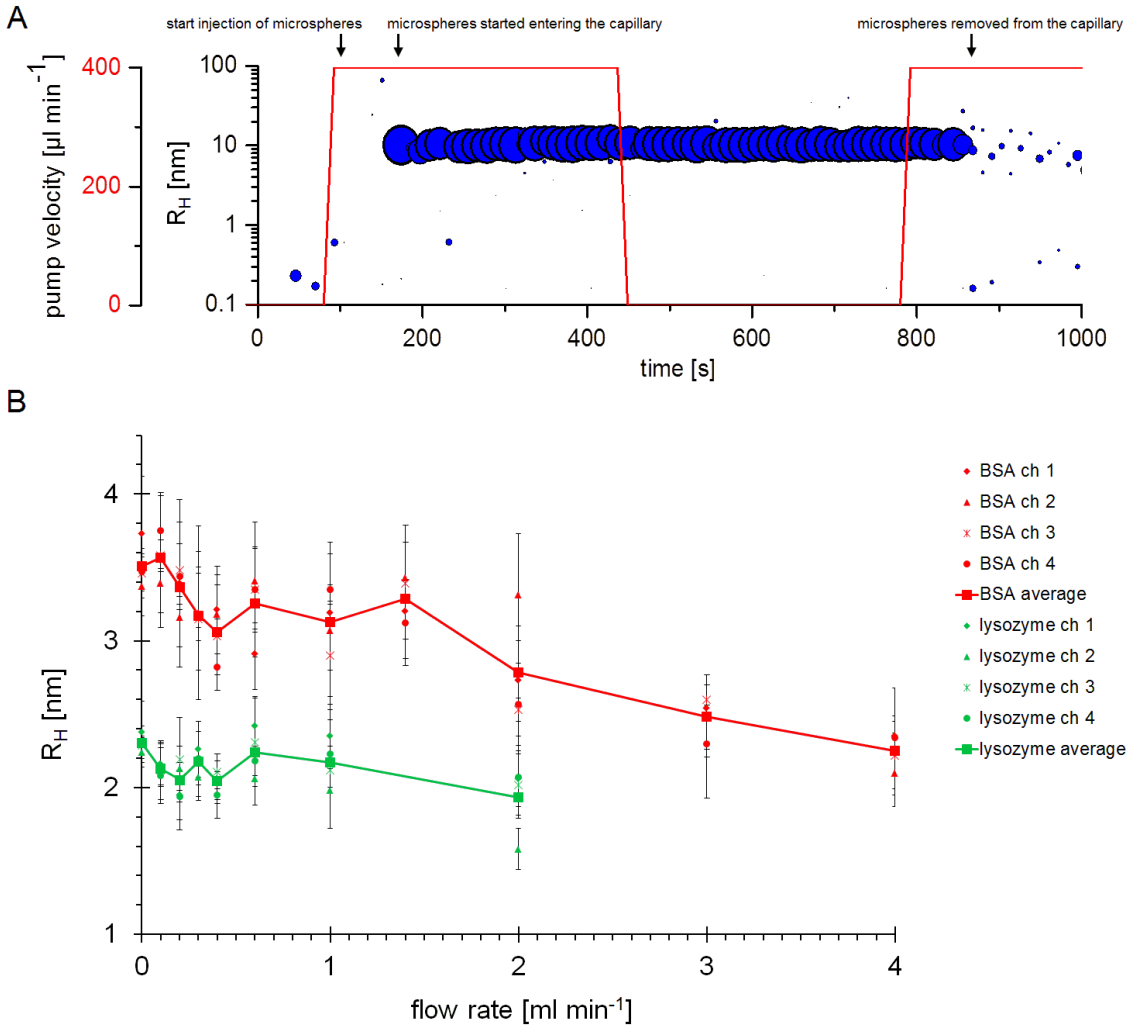

Figure 4 DLS experiments analyzing samples in flow. (**A**) A suspension of latex microspheres (R_H = 10.5 ± 0.5 nm, particle density: 20.6 mg cm^{-3}) was injected into a flexible tube attached to the capillary and maintained at a constant pump-driven velocity of 400 µl min^{-1} (red graph) to investigate the influence of the sample flow on the determined particle radius. After reaching the maximum intensity of light scattered by the microspheres, the pump was stopped for approx. 5 minutes. Finally, the pump was switched on again at the original flow rate of 400 µl min^{-1} (red graph) and the sample was washed out of the capillary. A hydrodynamic radius of 10.5 ± 0.7 nm was determined for the latex particles after averaging of the DLS data. The diameter of the blue spheres represents the relative abundance of the detected particle radii weighted by scattering intensities in arbitrary units.(**B**) BSA (9 mg ml^{-1}; 66 kDa) and lysozyme (16 mg ml^{-1}; 14 kDa) were analysed in a circular

flow tubing applying the four-channel *in situ* DLS instrument to systematically follow the radius determination at varying flow rates.

In the next step, we connected the lower end of a size-exclusion chromatography column to the sample capillary. This setup allows to characterize macromolecules by DLS inside the capillary directly after they eluted from the column. We applied a mixture of standard proteins to the column at a flow rate of 200 µl min^{-1} and again performed DLS continuously while the sample solution is flowing through the capillary (figure 5). The size and retention volume of the individual proteins is reliably resolved by the recorded count rate and radius plot as shown in figure 5A/B. The molecular weights range from 14 to 330 kDa for the respective monomeric protein. Moreover, the non-standard protein TCTP was applied to the SEC-DLS setup to further test the method, which revealed a predominantly dimeric state of the protein according to the retention volume and the DLS data (figure 6 and table 4).

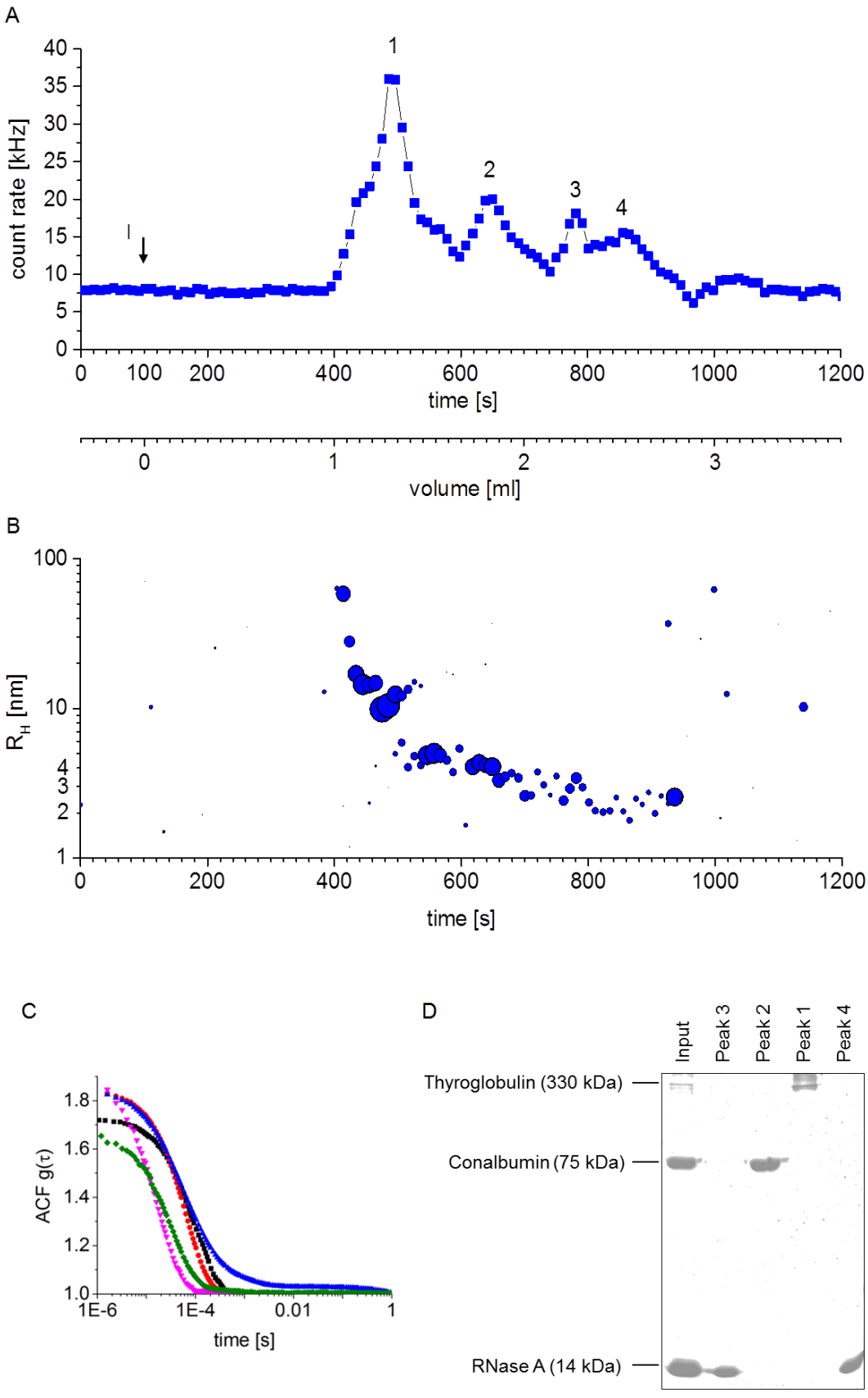
A
count rate [kHz]
time [s]
volume [ml]
1
2
3
4
I
B
R_H [nm]
time [s]
C
ACF g(τ)
time [s]
D
Input
Peak 3
Peak 2
Peak 1
Peak 4
Thyroglobulin (330 kDa)
Conalbumin (75 kDa)
RNase A (14 kDa)

Figure 5 Combined approach of *in situ* DLS and SEC: A mixture of thyroglobulin (3 mg ml^{-1}), conalbumin (7 mg ml^{-1}) and RNase A (15 mg ml^{-1}) after passing a Superdex 200 GL 5/150 column with a constant flow rate of 200 µl min^{-1}. Proteins in solution were instantly separated and individually analysed inside the capillary by *in situ* DLS. (**A**) The total scattering intensity (count rate; blue squares) of the solution is plotted against the retention time and volume of the column. After 100 s of DLS data recording the protein sample solution was injected ("I"). The observed void volume of the column corresponds to approx. 1 ml of retention volume. The obtained peaks were assigned to the individual proteins of the mixture, according to their specific elution properties and upon analysis by SDS-PAGE (Figure 5D). (**B**) In parallel, the time-course of the radius distribution (blue spheres) for the same experiment was recorded by DLS. Hydrodynamic radii of 9.5 nm (550 kDa), 4.2 nm (85 kDa) and 2.9 nm (35 kDa) and 2.0 nm (17 kDa) were determined for the peaks 1 to 4 in the respective chromatogram (Figure 5A). Therefore, the first peak was assigned to dimeric thyroglobulin (MW: 660 kDa), followed by monomeric conalbumin (MW: 75 kDa; peak 2) as well as dimeric (peak 3) and monomeric (peak 4) RNase A (MW of the monomer: 14 kDa). The diameter of the blue spheres represents the relative abundance of the detected particle radii weighted by scattering intensities in arbitrary units. (**C**) A set of ACFs is displayed comparatively. The average ACF of the putative thyroglobulin dimer peak (peak 1, figure 5A) determined by *in situ* DLS is shown in black. Further, the ACFs of thyroglobulin (red), conalbumin (green) and RNase A (magenta) are shown as obtained from a cuvette instrument, as well as the ACF for the mixture, determined by the same cuvette instrument (blue), for comparison and verification of the protein separation. (**D**) In order to confirm the protein content of the size-exclusion chromatography fractions (figure 5A), an aliquot of the identified count-rate peak fractions was subjected to SDS-PAGE analysis. The column input consisting of thyroglobulin, conalbumin and RNase A ("input") is shown for comparison of the molecular weights. Thereby, the identification of the proteins from peaks 1 to 4 based on the determined hydrodynamic radii (figure 5B) is confirmed by SDS-PAGE.

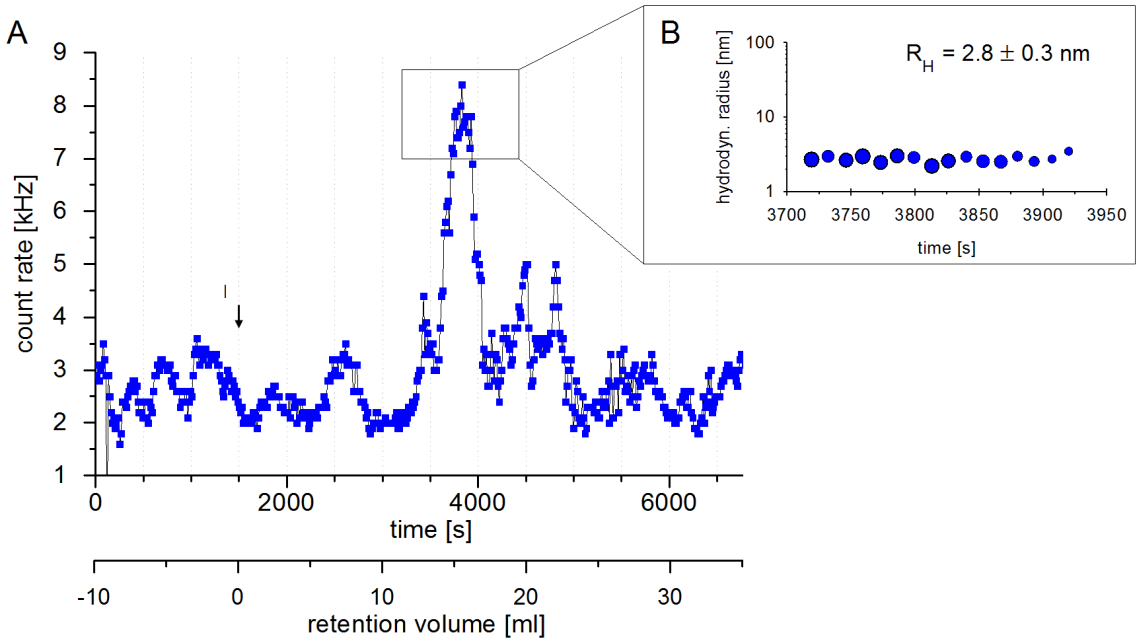

Figure 6 Combined approach of *in situ* DLS and SEC: TCTP (19 kDa; 5 mg ml^{-1}) in 100 µl buffer was applied to a Superdex 200 10/300 GL column and detected via DLS inside the sample capillary at a flow rate of 400 µl min^{-1}. A count rate peak was observed ($V_E \approx 15.5$ ml), that corresponds to a dimeric state, which is characterized by a hydrodynamic radius of 2.8 ± 0.3 nm. A highly similar value was determined by a DLS cuvette instrument (table 4). (**A**) The total scattering intensity (count rate; blue squares) of the solution is plotted against the retention volume of the column. The sample solution was injected at the time point labelled with "I". The indicated peak of TCTP is eluting after 15.5 ml corresponding to the expected molecular weight of around 38 kDa for a dimeric state. (**B**) The time-course of the hydrodynamic radius distribution for the highlighted peak from figure 7A. The radius of the blue spheres represents the relative abundance of the detected particle radii weighted by scattering intensities in arbitrary units.

3.2. Analysing sample dispersity by combined DLS and SAXS

The sample environment was designed to verify the dispersity of SAXS sample solutions immediately prior to the X-ray exposure by DLS and consider the results in SAXS data evaluation. Therefore, DLS and SAXS data of three standard proteins, namely RNase A (14 kDa), BSA (66 kDa) and apoferritin (440 kDa), were collected in parallel and evaluated as shown in figure 7A. In order to verify the quality of the data recorded in the new sample environment the obtained SAXS data sets were compared to the data deposited in the Small-Angle Scattering Biological Data Bank (SASBDB; Valentini et al., 2015), available via the entry codes SASDAR2, SASDA32 and SASDA82,

respectively. Additionally, the experimental SAXS data was compared to the solution scattering calculated from high-resolution structures as shown in figure 7A and table 5. DLS data displayed in figure 7B were collected right before the X-ray exposure. On the one hand SAXS data well correlates with expected values based on the respective SASBDB entries and is not affected by the DLS measurement and the attached DLS optics. On the other hand DLS also reliably determines the ACF and the hydrodynamic radius distribution of the applied sample solutions. All corresponding size and shape parameters are summarized in table 5.

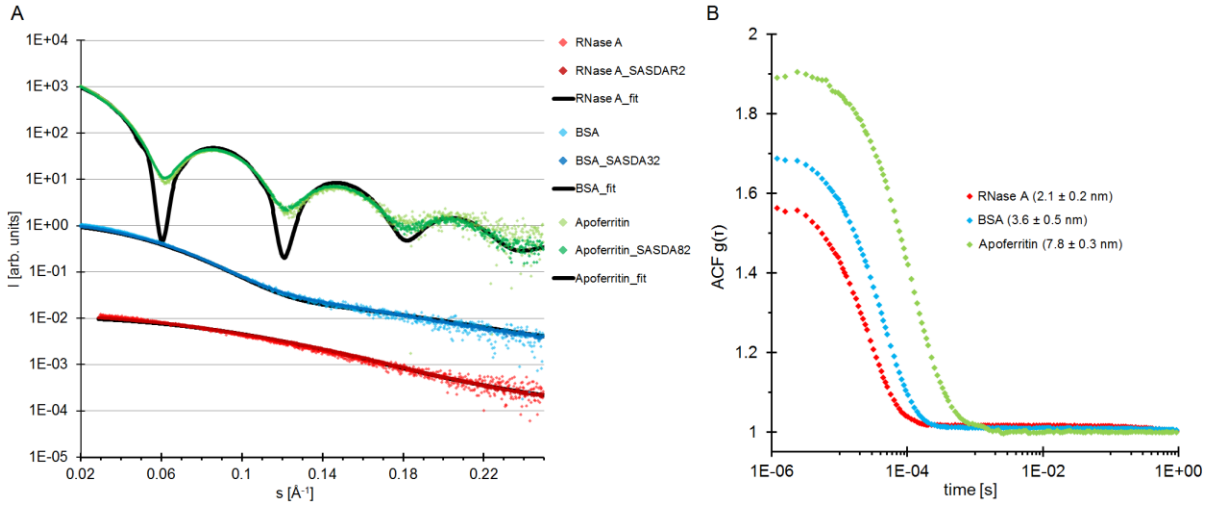

Figure 7 SAXS experiments combined with *in situ* DLS data collection to monitor particle size and to verify the SAXS data quality in the newly designed SEU. Scattering data of three standard proteins covering a wide molecular weight range are displayed. (**A**) Scattering intensities of RNase A (10 mg ml^{-1}), BSA (8 mg ml^{-1}) and apoferritin (5 mg ml^{-1}) were compared to the respective entries in the BioSAXS database SASBDB. The accompanying fit curve for each protein (black lines) calculated from the respective high-resolution structures is shown as well. The high similarity of the recorded SAXS data compared to previously collected data deposited in the database verifies that SAXS and DLS data can be collected in parallel applying the new implemented SEU. The scattering intensity values of each protein are displaced vertically for clarity (**B**) Averaged ACFs of the DLS data collected in parallel for the samples shown in figure 5A.

Table 5 Experimental results from combined DLS/SAXS experiments.

Sample (expected mass)	R_H [nm]	R_G [nm]	D_{max} [nm]	χ^2 (pdb code)[1]
RNase A (14 kDa)	2.0 ± 0.2	1.76 ± 0.17	5.0	1.542 (1C0B)
BSA (66 kDa)	3.5 ± 0.1	2.81 ± 0.17	9.1	6.140 (3V03)
Apoferritin (440 kDa; 24-mer)	7.8 ± 0.3	6.50 ± 1.65	14.3	6.708 (1IER)
*Tb*IMPDH (232 kDa; tetramer)	8.2 ± 0.2	5.21 ± 0.70	19.4	-

[1]χ^2-value of the optimized fit curve calculated from the pdb entry in brackets.

4. Discussion

Appropriate sample handling and preparation, including filtration and centrifugation of the samples is essential in order to remove undesired aggregates prior to SAXS measurements, to improve the precision of SAXS data and consequently to improve the accuracy of the derived structural models [Jeffries et al., 2016]. Aggregates in a protein solution, detectable by *in situ* DLS, commonly reduce the precision of molecular weight determination by SAXS and falsify the distance distribution function of the respective macromolecule. In this context a novel four-channel *in situ* DLS instrument was designed, constructed and adapted to the experimental sample exposure unit of the BioSAXS beamline P12. The DLS instrument is optimized to fit the SAXS sample environment and uses a novel expandable multi-channel approach for rapid data collection along the capillary cross-section and allows to perform DLS measurements inside the sample exposure unit in parallel to SAXS measurements. It thereby supports data evaluation and validation of SAXS experiments. DLS data recorded and information obtained by DLS will be implemented in the pipeline of SAXS data processing at EMBL beamline P12 [Franke et al., 2012]. To the best of our knowledge this is the first time that X-ray solution scattering data collection at a synchrotron source is combined with laser light scattering. Recently, a DLS laser probe was attached to a SAXS table top X-ray in order to characterize gold and latex nanoparticles. Nonetheless, this setup required much longer exposure times in comparison and was only capable of measuring at a very high scattering angle [Schwamberger et al., 2015].

The described multi-channel DLS system allows to detect inhomogeneities, which may arise for example from sample handling, heat or X-ray exposure. According to the example shown in figure 3 the new DLS instrument is able to monitor a shift of the radius distribution upon mixing a solution of lysozyme with minor amounts of BSA, which has approximately a two times higher R_H value and an exponentially increased intensity of scattered light. Specifically, the intensity of Rayleigh scattering depends on the sixth power of the particle diameter [Barnett, 1942], whereby large particles with a relative abundancy below 1% are detectable among smaller particles at a similar intensity level by the

DLS device, if the particle diameter differs by a factor of two to three. DLS also provides a complementary tool to follow the specific association and dissociation of oligomers. Limitations to identify polydispersity by DLS in mixtures of differently sized particles were till now only sparsely addressed, as for example by Karow et al. [2014].

Other methods that have been suggested more recently for complementary characterization and scoring of BioSAXS sample solutions are size-exclusion chromatography, mass spectrometry, analytical ultracentrifugation or native gel electrophoresis [Koch et al., 2013, Boivin et al., 2016]. However, all these methods require significantly more time and efforts compared to *in situ* DLS and some have a rather limited particle size range. SEC-SAXS, has been explored recently in several studies [Berthaud et al., 2012; Beckham et al., 2013; Pérez & Koutsioubas, 2015; Martino et al., 2016; Zhao et al., 2016] and was established at PETRA III beamline P12 by Graewert et al. [2015]. The method aims to instantaneously separate different particles by size before the sample solution is injected into the SAXS capillary. SEC-SAXS combinations are increasingly applied to improve SAXS data quality, particularly for biomolecules, which are in a rapid equilibrium of different oligomeric states. An additional biophysical characterization of the SEC-SAXS sample solution by static light scattering (SLS) was shown in the same study by Graewert et al. [2015]. However, this method requires to split the sample that is eluting from the SEC column in two fractions to prevent undesired band broadening. Utilizing the described DLS instrument the measurement takes place "on the spot" in the same compartment, which reduces band broadening and sample dilution to a minimum. Moreover, this sample characterization by DLS also allows to detect resin leaking from the SEC column as a result of the limited lifetime of SEC resins [Andersson, 2014].

We could demonstrate that DLS performed in a capillary subsequently after liquid chromatography provides additional and more accurate information about size, molecular weight and solution dispersity, as shown in figure 5. Specifically, in this setup the resolution of the particle size distribution and polydispersity by DLS is improved, the detected scattering of small particles is not diminished by larger particles in the sample solution, which allows a more precise size determination of the smaller particles by DLS and the option to directly verify the molecular weight via the retention volume. Moreover, the peak sizes of the individual separated particle species usually allow a rough estimation of the relative particle quantity.

Following this experiment, figure 6 is showing that this SEC-DLS approach is well applicable to determine the hydrodynamic radius and the putative dimerization of *At*TCTP, which has been uncharacterized so far. Particularly for larger complexes, the determination of the radius distribution by a combined SEC-DLS approach is most valuable to score sample solution, in some cases even beyond the separation limit of the used SEC column. A minor amount of large protein aggregates (R_H ≈ 20-60 nm), as evident from figure 5B and C, is frequently observed in mixtures of protein solutions

and was observed upon mixing of the applied proteins. Generally, such aggregates may result from unspecific protein-protein interaction in a concentration-dependent manner or arise from disulfide bonds as a result of oxidation or result from impurities that may have a low solubility in the applied buffer or an impurity that reduces the solubility of one of the proteins.

As the amount of photons focused into a volume fraction of a sample is reduced by exposing the sample in flow, measurements in flow mode are favored, if sufficient sample quantities are available. For most commonly used flow rates we could verify that continuous DLS measurements produce reliable data, as shown in figure 4. Further, the four-channel DLS system can be used to detect the concave meniscus of a sample suspension (figure 4A) and thereby provides information at which time point a sample suspension enters the SAXS sample container, as well as to verify the appropriate cleaning of the sample capillary in between exposures of different sample suspensions or solutions. However, in order to design advanced light-scattering-based instrumentation for beneficial sample characterization in flow, the laser should be tightly focused at the scattering volume fraction, because the laser diameter, next to the bulk flow velocity profile, affects the decay of the ACF of a diffusive process as found and practically verified by Taylor and Sorenson [1986]. In other words, a minimization of the time required for the particles to pass the scattering volume will improve the accuracy of the particle radius determination. In summary, the described novel multi-receiver DLS setup at the PETRA III BioSAXS beam line P12 allows most time-efficient sample scoring and supports SAXS data validation and interpretation.

Acknowledgements The authors acknowledge support by BMBF via project number 05K13GU2, and the Horizon 2020 programme of the European Union, iNEXT (H2020 Grant # 653706). SF is supported by the Hamburg Ministry of Science and Research via the graduate school DELIGRAH. MG was supported by the EMBL interdisciplinary Postdoc Programme under Marie Curie COFUND Actions. Many thanks to the staff of the SPC (EMBL-Hamburg) for their technical support. IMPDH and TCTP were kindly purified and provided by Nadine Werner (University Hamburg) and Steffen Pahlow (University Hamburg) respectively. The authors thank Robin Schubert (University Hamburg) for helpful discussion.

5. References

Andersson, M. (2014). *Digital Comprehensive Summaries of Uppsala Dissertations from the Faculty of Science and Technology 1202*. ISBN 978-91-554-9102-4.

Axelsson, I. & Heinegård, D. (1978). *Biochemical Journal*, **169**(3), 517–530.

Barnett, C. E. (1942). *J. Phys. Chem.*, **46**, 69-75.

Beckham, S. A., Brouwer, J., Roth, A., Wang, D., Sadler, A. J., John, M., Jahn-Hofmann, K., Williams, B., R., G., Wilce, J. A. & Wilce, M. C. J. (2013). *Nucleic Acids Research*, **41**, 3436–3445.

Berthaud, A., Manzi, J., Pérez, J. & Mangenot, S. (2012). *Journal of the American Chemical Society*, **134**, 10080–10088.

Blanchet, C. E., Spilotros, A., Schwemmer, F., Graewert, M. A., Kikhney, A., Jeffries, C. M., Franke, D., Mark, D., Zengerle, R., Cipriani, F., Fiedler, S., Roessle, M. & Svergun, D. I. (2015). *Journal of Applied Crystallography*, **48**, 431–443.

Boivin, S., Kozak, S., Rasmussen, G., Nemtanu, I. M., Vieira, V. & Meijers, R. (2016). *Methods*, **95**, 70–77.

Burchard, W., Frank, M. & Michel, E. (1996). *Berichte Der Bunsengesellschaft Für Physikalische Chemie*, **100**, 807–814.

Cantor, C. R. & Schimmel, P. R. (1980). *Biophysical Chemistry, Part II, New York, W. H. Freeman*.

Carvalho, J. W. P., Carvalho, F. A. O., Batista, T., Santiago, P. S. & Tabak, M. (2014). *Colloids and Surfaces B: Biointerfaces*, **118**, 14–24.

Chu, B. (1983). *The Application of Laser Light Scattering to the Study of Biological Motion*, pp. 53–76. Springer, Boston, MA.

Dahani, M., Barret, L.-A., Raynal, S., Jungas, C., Pernot, P., Polidori, A. & Bonneté, F. (2015). *Acta Crystallographica Section F Structural Biology Communications*, **71**, 838–846.

David, G. & Pérez, J. (2009). *Journal of Applied Crystallography*, **42**, 892–900.

Destremaut, F., Salmon, J.-B., Qi, L. & Chapel, J.-P. (2009). *Lab on a Chip*, **9**, 3289.

Edelhoch, H. & Lippoldt, R. E. (1960). *Journal of Biological Chemistry*, **235**(5), 1335–1340.

Fávero-Retto, M. P., Palmieri, L. C., Souza, T. A. C. B., Almeida, F. C. L. & Lima, L. M. T. R. (2013). *European Journal of Pharmaceutics and Biopharmaceutics*, **85**, 1112–1121.

Franke, D., Kikhney, A. G. & Svergun, D. I. (2012). *Nuclear Instruments and Methods in Physics Research Section A: Accelerators, Spectrometers, Detectors and Associated Equipment*, **689**, 52–59.

Franke, D., Petoukhov, M. V., Konarev, P. V., Panjkovich, A., Tuukkanen, A., Mertens, H. D. T., Kikhney, A. G., Hajizadeh, N. R., Franklin, J. M., Jeffries, C. M. & Svergun, D. I. (2017). *Journal of Applied Crystallography*, **50**, 1212–1225.

Frankema, W., van Bruijnsvoort, M., Tijssen, R. & Kok, W. T. (2002). *Journal of Chromatography. A*, **943**, 251–261.

Gast, K., Noeppert, A., Müller-Frohne, M., Zirwer, D. & Damaschun, G. (1997). *European Biophysics Journal*, **25**, 211–219.

Georgieva, D., Koker, M., Redecke, L., Perbandt, M., Clos, J., Bredehorst, R., Genov, N. & Betzel, C. (2004). *Biochemical and Biophysical Research Communications*, **323**, 1278–1286.

Graewert, M. A., Franke, D., Jeffries, C. M., Blanchet, C. E., Ruskule, D., Kuhle, K., Flieger, A., Schäfer, B., Tartsch, B., Meijers, R. & Svergun, D. I. (2015). *Scientific Reports*, **5**, 10734.

Graceffa, R., Nobrega, R. P., Barrea, R. A., Kathuria, S. V., Chakravarthy, S., Bilsel, O., & Irving, T. C. (2013). *Journal of Synchrotron Radiation*, **20**, 820–825.

Jeffries, C. M., Graewert, M. A., Svergun, D. I. & Blanchet, C. E. (2015). *Journal of Synchrotron Radiation*, **22**, 273–279.

Jeffries, C. M., Graewert, M. A., Blanchet, C. E., Langley, D. B., Whitten, A. E. & Svergun, D. I. (2016). *Nature Protocols*, **11**, 2122–2153.

Karow, A. R., Götzl, J. & Garidel, P. (2015). *Pharmaceutical Development and Technology*, **20**, 84–89.

Khan, S., Birch, J., Harris, P., Van Calsteren, M.-R., Ipsen, R., Peters, G. H. J., Svensson, B. & Almdal, K. (2017). *Biomacromolecules*, **18**, 747–756.

Koch, C., Tria, G., Fielding, A. J., Brodhun, F., Valerius, O., Feussner, K., Braus, G. H., Svergun, D. I., Bennati, M. & Feussner, I. (2013). *Biochimica Et Biophysica Acta*, **1831**, 1449–1457.

Lee, J., Wu, W., Jiang, J. Y., Zhu, B. & Boas, D. A. (2012). *Optics Express*, **20**, 22262–22277.

Leung, A. B., Suh, K. I. & Ansari, R. R. (2006). Applied Optics, **45**, 2186–2190.

Liu, J., Falke, S., Drobot, B., Oberthuer, D., Kikhney, A., Guenther, T., Fahmy, K., Svergun, D. I., Betzel, C. & Raff, J. (2017). *European Biophysics Journal*, **46**, 77–89.

Loske, A. M., Tello, E. M., Vargas, S. & Rodriguez, R. (2014). *Archives of Microbiology*, **196**, 557–563.

Maes, D., Vorontsova, M. A., Potenza, M. A. C., Sanvito, T., Sleutel, M., Giglio, M. & Vekilov, P. G. (2015). *Acta Crystallographica. Section F, Structural Biology Communications*, **71**, 815–822.

Martin, H. P., Brooks, N. J., Seddon, J. M., Luckham, P. F., Terrill, N. J., Kowalski, A. J. & Cabral, J. T. (2016). *Soft Matter*, **12**, 1750–1758.

Martino, L., Holland, L., Christodoulou, E., Kunzelmann, S., Esposito, D. & Rittinger, K. (2016). *PloS One*, **11**, e0164662.

Mikol, V., Hirsch, E. & Giegé, R. (1989). *FEBS Letters*, **258**, 63–66.

Minton, A. P. (2016). *Analytical Biochemistry*, **501**, 4–22.

Meyer, A., Dierks, K., Hilterhaus, D., Klupsch, T., Mühlig, P., Kleesiek, J., Schoepflin, R., Einspahr, H., Hilgenfeld, R. & Betzel, C. (2012). *Acta Crystallographica Section F Structural Biology and Crystallization Communications*, **68**, 994–998.

Meyer, A., Dierks, K., Hussein, R., Brillet, K., Brognaro, H. & Betzel, C. (2015). *Acta Crystallographica Section F Structural Biology Communications*, **71**, 75–81.

Noeppert, A., Gast, K., Müller-Frohne, M., Zirwer, D. & Damaschun, G. (1996). *FEBS Letters*, **380**, 179–182.

Oberthuer, D., Melero-García, E., Dierks, K., Meyer, A., Betzel, C., Garcia-Caballero, A. & Gavira, J. A. (2012). *PLoS ONE*, **7**, e33545.

Passow, C., Hagen, B. ten, Löwen, H. & Wagner, J. (2015). *The Journal of Chemical Physics*, **143**, 44903.

Popov, I. & Vitkin, A. (2016). *Journal of Biomedical Optics*, **21**, 17002.

Pérez, J. & Koutsioubas, A. (2015). *Acta Crystallographica Section D: Biological Crystallography*, **71**, 86–93.

Poulos, A. S., Nania, M., Lapham, P., Miller, R. M., Smith, A. J., Tantawy, H., Caragay, J., Gummel, J., Ces, O., Robles, E. S. J. & Cabral, J. T. (2016). *Langmuir: The ACS Journal of Surfaces and Colloids*, **32**, 5852–5861.

Provencher, S. W. (1982). *Computer Physics Communications*, **27**, 229–242.

Round, A., Felisaz, F., Fodinger, L., Gobbo, A., Huet, J., Villard, C., Blanchet, C., Pernot, P., McSweeney, S., Roessle, M., Svergun, D. I. & Cipriani, F. (2015). *Acta Crystallographica Section D: Biological Crystallography*, **71**, 67–75.

Regini, J. W., Ecroyd, H., Meehan, S., Bremmell, K., Clarke, M. J., Lammie, D., Wess, T. & Carver, J. A. (2010). *Molecular Vision*, **16**, 2446–2456.

Schubert, R., Meyer, A., Dierks, K., Kapis, S., Reimer, R., Einspahr, H., Perbandt, M. & Betzel, C. (2015). *Journal of Applied Crystallography*, **48**, 1476–1484.

Schubert, R., Meyer, A., Baitan, D., Dierks, K., Perbandt, M. & Betzel, C. (2017). *Crystal Growth & Design*, 17, 3579–3579.

Schwamberger, A., De Roo, B., Jacob, D., Dillemans, L., Bruegemann, L., Seo, J. W. & Locquet, J. P. (2015). *Nuclear Instruments and Methods in Physics Research Section B: Beam Interactions with Materials and Atoms*, **343**, 116–122.

Svergun, D., Barberato, C. & Koch, M. H. J. (1995). *Journal of Applied Crystallography*, **28**, 768–773.

Sviridova, E., Rezacova, P., Bondar, A., Veverka, V., Novak, P., Schenk, G., Svergun, D. I., Smatanova, I. K. & Bumba, L. (2017). *Scientific Reports*, **7**, 40408.

Taylor, T.W., Sorensen, C.M. (1986). *Appl. Opt.*, **25**, 2421–2426.

Tuukkanen, A. T., Kleywegt, G. J. & Svergun, D. I. (2016). *IUCrJ*, **3**, 440–447.

Valentini, E., Kikhney, A.G., Previtali, G., Jeffries, C.M. & Svergun, D.I. (2015). *Nucleic Acids Res.* **28**, 357–63.

Wong, K. K. W., Douglas, T., Gider, S., Awschalom, D. D. & Mann, S. (1998). *Chemistry of Materials*, **10**, 279–285.

Yang, Y., Heo, P., Kong, B., Park, J.-B., Jung, Y.-H., Shin, J., Jeong, C. & Kweon, D.-H. (2015). *Biochemical and Biophysical Research Communications*, **465**(4), 864–870.

Zhao, H., Speir, J. A., Matsui, T., Lin, Z., Liang, L., Lynn, A. Y., Varnado B., Weiss, T. M. & Tang, L. (2016). *PLOS ONE*, **11**, e0149337.